Dyes and Pigments 156 (2018) 369–378

Contents lists available at ScienceDirect

Dyes and Pigments

journal homepage: www.elsevier.com/locate/dyepig

Blue light emission of new anthracene derivatives produced using optimized side group link positions

Seokwoo Kang[a], Hyocheol Jung[a], Hayoon Lee[a], Suji Lee[b], Mina Jung[b], Jaehyun Lee[b], Young Chul Kim[a], Jongwook Park[a,*]

[a] Department of Chemical Engineering, Kyunghee University, Gyeonggi, 17104, South Korea
[b] Department of Chemistry, The Catholic University, South Korea

ABSTRACT

Using an anthracene chromophore as a core group and a phenyl carbazole chromophore as a side group, three new emitters of blue light, 2-DCPA, 3-DCPA and 4-DCPA, were synthesized. The three compounds differed with regard to the position of the carbazole linked to the core, with 2-DCPA and 4-DCPA using carbazole nodes and 3-DCPA using the lobe position. Density functional theory calculations were performed to determine which positions of the carbazole moiety had node characteristics and which had lobe characteristics. The PL_{max} values of 2-DCPA, 3-DCPA and 4-DCPA in the film state were in the blue region, at 453, 457, and 452 nm, respectively. Of these materials, 3-DCPA, i.e., that with the linkage to the lobe position, showed the highest efficiency, with a value of 2.91 cd/A, and EQE, with a value of 2.65%. In a doped device using CBP as a host material and 3-DCPA as a dopant, the EL_{max} emission was observed to be in the deep blue region, at 433 nm, and with a CIE value of (0.150, 0.068).

1. Introduction

Organic light-emitting diodes (OLEDs) were first reported by Tang and Van Slyke, and are now attracting attention in the market, for applications such as mobile phones, television displays and solid-state lighting, because of their potential as next-generation devices [1]. OLED device emits light which comes from exciton in the emission material layer (EML), and the exciton is produced from electrons and holes which are injected at the cathode and anode. In here, emitting material plays an important role in determining the wavelength and efficiency of the OLEDs.

Therefore, to achieve high performance of full-color OLED display, it is necessary to develop red, green, and blue emitting materials having high efficiency and long life-time [2–4]. In particular, in case of a blue emitting material for a television display, the Commission Internationale de L'Eclairage coordinates CIE (x, y) of (0.14, 0.08) is required by the National Television System Committee (NTSC), and CIX (x, y) of (0.15, 0.06) is required for a deep blue material of high-definition television (HDTV) [5]. However, blue light-emitting materials require a wide energy band gap, which causes high charge injection barriers in the device, and thus blue OLED devices are inferior to green and red ones in terms of electroluminescence (EL) efficiency and device life-time [6–12]. Many studies have been carried out to introduce various side groups that effectively prevent intermolecular packing and increase the electroluminescence (EL) efficiency of blue light-emitting core chromophores having high photoluminescence (PL) efficiency such as anthracene, pyrene and chrysene [13–15].

In this study, we used density functional theory (DFT) to determine the location of orbital nodes and lobes within a core-side framework. The selected side group was designed to contain the carbazole moiety, since this moiety has been shown to contribute to good charge transport and high PL efficiency [16]. In addition, a phenyl group was introduced into the side group in order to block the carbazole NH group quenching site and to add effects resulting from having a bulky chemical structure [17]. DFT calculations showed the 2 and 4 positions of the carbazole to have node characteristics, and the 3 position to have lobe characteristics. Using these three different positions, we synthesized three new compounds, namely 9,10-bis(9-phenyl-9H-carbazol-2-yl)anthracene (2-DCPA), 9,10-bis(9-phenyl-9H-carbazol-3-yl)anthracene (3-DCPA), and 9,10-bis(9-phenyl-9H-carbazol-4-yl)anthracene (4-DCPA) as shown in Scheme 1.

* Corresponding author.
E-mail address: jongpark@khu.ac.kr (J. Park).

https://doi.org/10.1016/j.dyepig.2018.04.029
Received 19 March 2018; Received in revised form 15 April 2018; Accepted 16 April 2018
Available online 18 April 2018

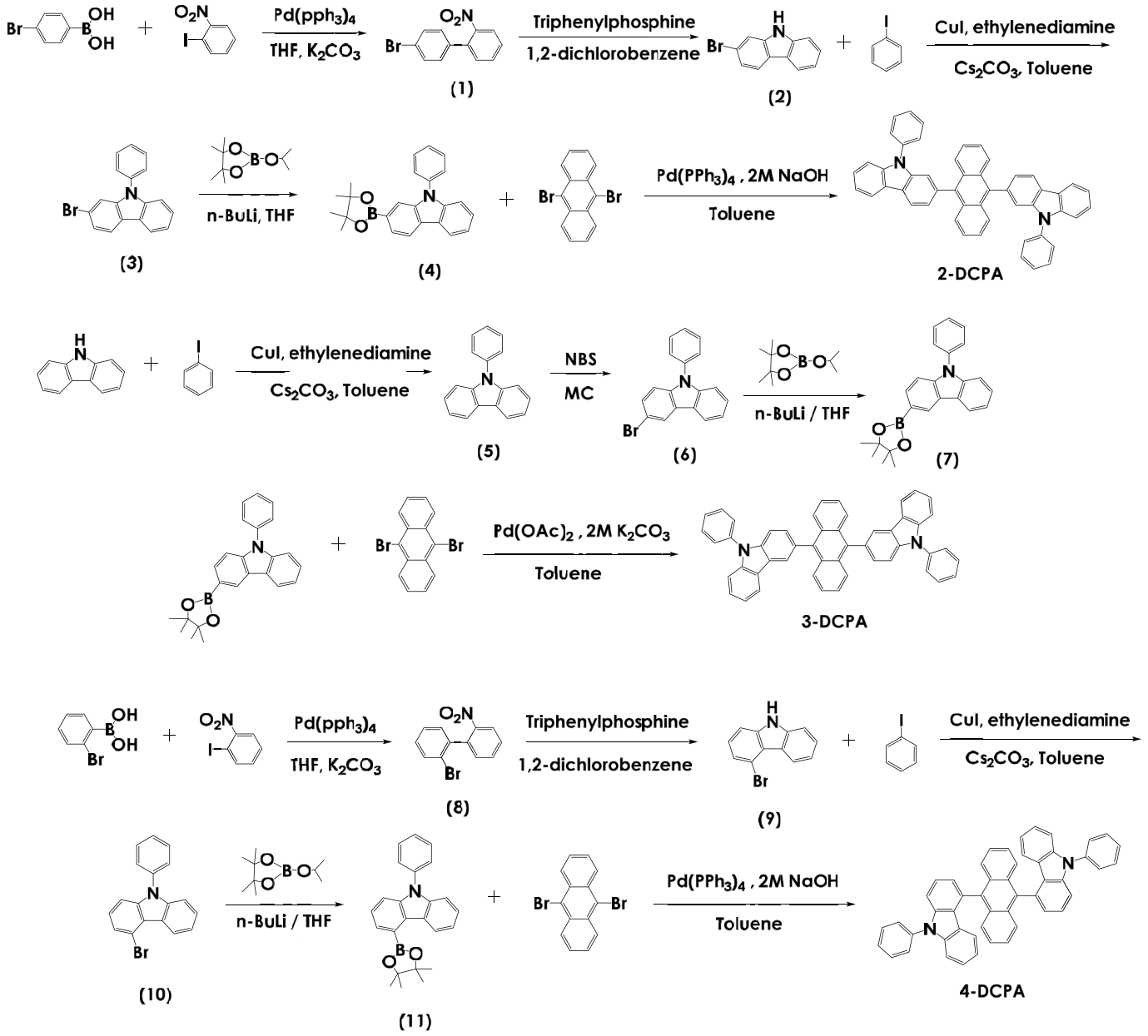

Scheme 1. Synthetic routes to 2-DCPA, 3-DCPA, and 4-DCPA.

2. Experimental

2.1. Synthesis

Compound (1) 4′-bromo-2-nitro-biphenyl 4-bromophenylboronic acid (12.9 g, 64.7 mmol), 1-Iodo-2-nitro-benzene (10.0 g, 49.7 mmol), $Pd(pph_3)_4$ (2.9 g, 2.5 mmol) were added to 120 mL of anhydrous THF solution in 3-neck round bottom flask under N_2 atmosphere. Then, 60 mL of 2M K_2CO_3 was added to the reaction mixture. The mixture was heated 80 °C for 1 day under N_2 atmosphere. (7.5 g, Yield 60%) ^{1}H NMR (300 MHz, THF): δ(ppm) 7.93–7.90 (d, 1H), 7.70–7.65 (t, 1H), 7.60–7.53 (m, 3H), 7.49–7.47 (d, 1H), 7.27–7.26 (t, 1H), 7.24–7.23 (t, 1H).

Compound (2) 2-bromo-9H-carbazole 4′-bromo-2-nitro-biphenyl (5.9 g, 21.3 mmol), triphenylphosphine (13.96 g, 53 mmol) were added to 70 mL of anhydrous 1,2-diclorobenzene solution in 3-neck round bottom flask under N_2 atmosphere. The mixture was refluxed at 180 °C for 10 h (3.27 g, Yield 56%) ^{1}H NMR (300 MHz, THF): δ(ppm) 10.45 (s, 1H), 8.04–8.01 (d, 1H), 7.96–7.94 (d, 1H), 7.57 (s, 1H), 7.42–7.32 (m, 2H), 7.27–7.24 (d, 1H), 7.17–7.11 (t, 1H).

Compound (3) 2-bromo-9-phenyl-9H-carbazole 2-bromo-9H-carbazole (2 g, 8 mmol), copper(I) iodide (1.24 g, 6.5 mmol), cesium carbonate (7.98 g, 24 mmol) were added to 25 mL of anhydrous toluene solution in 3-neck round bottom flask under N_2 atmosphere. After the mixture was heated at 80 °C, iodobenzene (1.82 mL, 16 mmol), ethylenediamine (0.82 mL, 12.2 mmol) was added to mixture. Then the mixture was refluxed at 110 °C for 15 h ^{1}H NMR (300 MHz, THF): δ(ppm) 8.14–8.11 (d, 1H), 8.07–8.04 (d, 1H), 7.67–7.62 (m, 2H), 7.59–7.56 (m, 2H), 7.53–7.47 (m, 2H), 7.39–7.32 (m, 3H), 7.27–7.21 (t, 1H).

Compound (4) 2-boro-9-phenyl-9H-carbazole 2-bromo-9-phenyl-9H-carbazole (2.27 g, 7 mmol) was dissolved in 100 mL of anhydrous THF solution and cooled to −78 °C. Then, 7.07 mL of 2.0 M *n*-butyllithium (14 mmol) was slowly added dropwise. After the mixture was stirred at −78 °C for 30 min, 4 mL of 2-Isopropoxy-4,4,5,5-tetramethyl-1,3,2-dioxa-borolane (21 mmol) was slowly added. The resulting mixture was stirred for 3 h and gradually allowed to warm to room temperature. After the reaction was finished, the reaction mixture was extracted with ethyl acetate and water. The organic layer was dried with anhydrous $MgSO_4$ and filtered. The solvent was vaporized and recrystallized using hexane. (1.9 g, Yield 70%) ^{1}H NMR (300 MHz, THF): *δ*(ppm) 8.17–7.81 (t, 2H), 7.79 (s, 1H), 7.69–7.62 (t, 2H), 7.60–7.56 (t, 3H), 7.52–7.46 (t, 1H), 7.40–7.33 (m, 2H), 7.25–7.20 (t, 1H), 1.31 (s, 12H).

9,10-bis(9-phenyl-9H-carbazol-2-yl)anthracene (2-DCPA) 9,10-dibromoanthracene (1.0 g, 2.6 mmol), 2-boro-9-phenyl-9H-carbazole (2.5 g, 6.5 mmol), $Pd(PPh_3)_4$ (0.3 g, 0.2 mmol) were added to 25 mL of anhydrous toluene under N_2 atmosphere and stirred. 12 mL of tetraethylammonium hydroxide (20 wt %) was added to the mixture and stirred for reflux at 110 °C. After 2 h of reaction, the crude solution was filtered and the solvent of residue was vaporized. (0.4 g, Yield: 40%) ^{1}H NMR (300 MHz, THF): *δ*(ppm) 8.42–8.38 (t, 1H), 8.30–8.27 (d, 1H), 7.70–7.60 (m, 4H), 7.57–7.30 (m, 8H), 7.22–7.26 (q, 2H). HRMS (FAB-MS, *m/z*): calcd. for C50H32N2, 660.26; found, 660.2578 [M] + . Anal. calcd for C50H32N2: C 90.88, H 4.88, N 4.24; found: C 90.58, H 4.67 N 4.19%.

Compound (5) 9-phenyl-9H-carbazole 9H-carbazole (10 g, 60 mmol), copper(I) iodide (9.1 g, 48 mmol), cesium carbonate (58.4 g, 180 mmol) were added to 90 mL of anhydrous toluene solution in 3-neck round bottom flask under N_2 atmosphere. After the mixture was heated at 80 °C, iodobenzene (13.3 mL, 120 mmol), ethylenediamine (6 mL, 18 mmol) was added to mixture. Then the mixture was refluxed at 110 °C for 15 h (8.8 g, Yield 60%) ^{1}H NMR (300 MHz, DMSO): *δ*(ppm) 8.27–8.24 (d, 2H), 7.72–7.66 (t, 2H), 7.64–7.61 (d, 2H), 7.57–7.52 (t, 1H), 7.47–7.41 (t, 2H), 7.39–7.36 (d, 2H), 7.32–7.30 (t, 2H).

Compound (6) 3-bromo-9-phenyl-9H-carbazole 9-phenyl-9H-carbazole (6 g, 27 mmol), *N*-Bromosuccinimide (4.3 g, 27 mmol) were added to 30 mL of chloroform solution in 3-neck round bottom flask and stirred for 30 min at room temperature. After vaporizing the solvent, the crude product was recrystallized using hexane. (7.4 g, Yield 85%) ^{1}H NMR (300 MHz, $CDCl_3$): *δ*(ppm) 8.25–8.24 (d, 1H), 8.10–8.07 (d, 1H), 7.64–7.58 (t, 2H), 7.54–7.45 (m, 4H), 7.44–7.37 (m, 2H), 7.32–7.27 (m, 2H).

Compound (7) 3-boro-9-phenyl-9H-carbazole 3-bromo-9-phenyl-9H-carbazole (5 g, 15 mmol) was dissolved in 75 mL of anhydrous THF solution and cooled to −78 °C. Next, 10 mL of 2 M *n*-butyllithium (16.5 mmol) was slowly added dropwise. After the mixture was stirred at −78 °C for 30 min, 2.2 mL of 2-Isopropoxy-4,4,5,5-tetramethyl-1,3,2-dioxa-borolane (19 mmol) was slowly added. The resulting mixture was stirred for 3 h and gradually allowed warm to room temperature. After the reaction was completed, the crude product was extracted using ethyl acetate and D.I water. Water remaining in the organic layer is removed using anhydrous magnesium sulfate. The solvent was vaporized and recrystallized using hexane. (3.65 g, Yield 68%) ^{1}H NMR (300 MHz, $CDCl_3$): *δ*(ppm) 8.64 (s, 1H), 8.19–8.16 (d, 1H), 7.87–7.84 (d, 1H), 7.63–7.54 (m, 4H), 7.54–7.49 (t, 1H), 7.40–7.35 (m, 3H), 7.31–7.28 (d, 1H), 1.40 (s, 12H).

9,10-bis(9-phenyl-9H-carbazol-3-yl)anthracene (3-DCPA) 9,10-dibromoanthracene (1.3 g, 3.9 mmol), 3-boro-9-phenyl-9H-carbazole (3.0 g, 8.1 mmol), $Pd(OAc)_2$ (0.08 g, 0.4 mmol), tricyclohexylphosphine (0.2 g, 0.8 mmol) were added to 20 mL of anhydrous toluene solution in 3-neck round bottom flask under N_2 atmosphere. After the mixture was heated at 80 °C, 8 mL of 2 M potassium carbonate was added to mixture. Then the mixture was refluxed at 110 °C for 2 h (0.65 g, Yield 57%) ^{1}H NMR (300 MHz, THF): *δ*(ppm) 8.31–8.29 (d, 2H), 8.18–8.14 (t, 2H), 7.81–7.65 (m, 14H), 7.57–7.48 (m, 6H), 7.46–7.40 (t, 2H), 7.31–7.23 (m, 6H). HRMS (FAB-MS, *m/z*): calcd. for C50H32N2, 660.26; found, 660.2631 [M] + . Anal. calcd for C50H32N2: C 90.88, H 4.88, N 4.24; found: C 90.66, H 4.90 N 4.22%.

Compound (8) 2′-bromo-2-nitro-biphenyl 2-bromophenylboronic acid (10 g, 50 mmol), 1-Iodo-2-nitro-benzene (9 g, 45 mmol), $Pd(pph_3)_4$ (2.6 g, 4.5 mmol) were added to 120 mL of anhydrous THF solution in 3-neck round bottom flask under N_2 atmosphere. Next, 60 mL of 2M K_2CO_3 was added to the reaction mixture and then heated 80 °C for 1 day under N_2 atmosphere. After vaporizing the solvent, the crude product was recrystallized using hexane. (8.0 g, Yield 75%) ^{1}H NMR (300 MHz, THF): *δ*(ppm) 8.12–8.09 (d, 1H), 7.76–7.70 (t, 1H), 7.66–7.59 (m, 2H), 7.43–7.37 (t, 2H), 7.30–7.25 (t, 2H).

Compound (9) 4-bromo-9H-carbazole 2′-bromo-2-nitro-biphenyl (7 g, 26 mmol), triphenylphosphine (16.7 g, 65 mmol) were added to 60 mL of anhydrous 1,2-diclorobenzene solution in 3-neck round bottom flask under N_2 atmosphere. The mixture was refluxed at 180 °C for 10 h (3.0 g, Yield 50%) ^{1}H NMR (300 MHz, THF): *δ*(ppm) 10.58 (s, 1H), 8.65–8.62 (d, 1H), 7.45–7.36 (m, 3H), 7.31–7.29 (d, 1H), 7.23–7.15 (m, 2H).

Compound (10) 4-bromo-9-phenyl-9H-carbazole 4-bromo-9H-carbazole (2 g, 8 mmol), copper(I) iodide (1.24 g, 6.5 mmol), cesium carbonate (7.98 g, 24 mmol) were added to 25 mL of anhydrous toluene solution in 3-neck round bottom flask under N_2 atmosphere. After the mixture was heated at 80 °C, iodobenzene (1.82 mL, 16 mmol), ethylenediamine (0.82 mL, 12.2 mmol) was added to mixture. Then the mixture was refluxed at 110 °C for 15 h (1.7 g, Yield 68%) ^{1}H NMR (300 MHz, THF): *δ*(ppm) 8.81–8.78 (d, 1H), 7.65–7.59 (t, 2H), 7.56–7.47 (m, 3H), 7.45–7.40 (m, 2H), 7.35–7.27 (q, 3H), 7.25–7.20 (t, 1H).

Compound (11) 4-boro-9-phenyl-9H-carbazole 4-bromo-9-phenyl-9H-carbazole (1.5 g, 4.7 mmol) was dissolved in 72 mL of anhydrous THF solution and cooled to −78 °C. Next, 4.7 mL of 2 M *n*-butyllithium (9.4 mmol) was slowly added dropwise. After the mixture was stirred at −78 °C for 30 min, 2.77 mL of 2-Isopropoxy-4,4,5,5-tetramethyl-1,3,2-dioxa-borolane (14 mmol) was slowly added. The resulting mixture was stirred for 3 h and gradually allowed warmed to room temperature. After the reaction was completed, the crude product was extracted using ethyl acetate and D.I water. Water remaining in the organic layer is removed using anhydrous magnesium sulfate. The solvent was vaporized and recrystallized using hexane. (1.0 g, Yield 63%) ^{1}H NMR (300 MHz, DMSO): *δ*(ppm) 1.44(s, 12H), 7.24–7.31(m, 2H), 7.39–7.46(q, 3H), 7.54–7.58(q, 3H), 7.66–7.72(m, 3H), 8.96–8.99(d, 1H).

9,10-bis(9-phenyl-9H-carbazol-4-yl)anthracene (4-DCPA) 9,10-dibromoanthracene (0.7 g, 1.8 mmol), 4-boro-9-phenyl-9H-carbazole (1.8 g, 4.5 mmol), $Pd(PPh_3)_4$ (0.21 g, 0.14 mmol) were added to 40 mL of anhydrous toluene under N_2 atmosphere and stirred. 9 mL of tetraethylammonium hydroxide (20 wt%) was added to the mixture and stirred for reflux at 110 °C. After 2 h of reaction, the crude solution was filtered and the solvent of residue was vaporized. (0.35 g, Yield: 46%) ^{1}H NMR (300 MHz, DMSO): *δ*(ppm) 6.30–6.32(d, 1H), 6.72–6.78(t, 1H), 7.27–7.45(m, 5H), 7.60–7.67(m, 4H), 7.73–7.83(m, 5H). HRMS (FAB-MS, *m/z*): calcd. for C50H32N2, 660.26; found, 660.2565 [M] + . Anal. calcd for C50H32N2: C 90.88, H 4.88, N 4.24; found: C 90.71, H 4.82 N 4.09%.

2.2. General procedure of compound purification

All intermediate compounds from compound (1) to (11) except compound (4), (7), and (11) as well as final compounds of 2-DCPA, 3-DCPA, and 4-DCPA were purified by the following method: After the reaction was completed, the crude product was extracted by using methylene chloride (MC) and deionized water. Water remaining in the organic layer is removed by using anhydrous magnesium sulfate.

Recrystallization was proceeded by using hexane solvent for the

compounds of (1), (4), (6), (7), (8), and (11). Compounds of (2), (3), (5), (9), (10), 2-DCPA, 3-DCPA, and 4-DCPA were purified by silica gel chromatography having the moving solvent conditions: MC: hexane = 1: 3 for (2) and (9), MC: hexane = 1: 4 for (3), (5), and (10), chloroform: cyclohexane = 1: 4 for 2-DCPA and 4-DCPA, chloroform: hexane = 1: 3 for 3-DCPA.

2.3. Measurements and OLED fabrication

Reagents and solvents were purchased from Sigma Aldrich and Alfa aesar without further purification. Analytical TLC was performed on Merck 60 F254 silica gel plate, and column chromatography was performed on Merck 60 silica gel (230–400 mesh). The ^{1}H NMR spectra were recorded on Bruker Avance 300 spectrometers. The FAB + -mass and EI + -spectra were recorded on a JMS-600W, JMS-700, 6890 Series and Flash1112, Flash2000. The optical UV-Vis absorption spectra were obtained using a Lambda 1050 UV/Vis/NIR spectrometer (Perkin Elmer). A Perkin-Elmer luminescence spectrometer LS55 (Xenon flash tube) was used to perform PL spectroscopy. The glass transition temperatures (T_g) of synthesized materials were differential scanning calorimetry (DSC) under a nitrogen atmosphere using a DSC 4000 (Perkin Elmer). T_d of the compounds were measured with thermal gravimetric analysis (TGA) using a TGA4000 (Perkin Elmer). The HOMO energy levels were determined with ultraviolet photoelectron yield spectroscopy (Riken Keiki AC-2). The LUMO energy levels were derived from the HOMO energy levels and the band gaps. For the EL devices, all organic layers were deposited under 10^{-6} torr, with a rate of deposition of 1 Å/s to give an emitting area of 4 mm^2. The LiF and aluminum layers were continuously deposited under the same vacuum conditions. The current-voltage-luminance (I-V-L) characteristics of the fabricated EL devices were obtained with a Keithley 2400 electrometer. Light intensities were obtained with a Minolta CS-1000A. The operational stabilities of the devices were measured under encapsulation in a glovebox.

3. Results and discussion

3.1. Molecular design and synthesis

Three compounds, namely 2-DCPA, 3-DCPA, and 4-DCPA, were synthesized by carrying out Suzuki aryl-aryl coupling reactions as shown in Fig. 1 and Scheme 1. 9,10-dibromoanthracene and three boronyl compounds, specifically *N*-phenyl-2-carbazole boronate, *N*-phenyl-3-carbazole boronate, and *N*-phenyl-4-carbazole boronate, were used for the final syntheses. The expected structures of the synthesized compounds were confirmed by performing nuclear magnetic resonance (NMR) spectroscopy, elemental analysis (EA), and fast atom bombardment (FAB) mass analysis.

The position of the phenyl carbazole side group linked to the anthracene core differed for the three synthesized compounds, being the 3-position lobe site of the carbazole moiety for 3-DCPA and the 2- and 4-position node sites of the carbazole moiety for 2-DCPA and 4-DCPA,

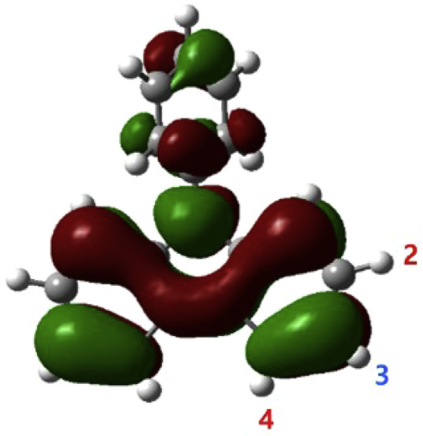

Fig. 2. Electron distribution density of carbazole.

respectively. As shown in Fig. 2, our DFT calculations produced an electron density distribution of phenyl carbazole showing the 3-position of the carbazole to be rich in electrons and the 2- and 4- positions of the carbazole to be deficient in electron density. When a side group donates electrons to a core anthracene chromophore, the electroluminescence (EL) efficiency of the compound is generally increased. Thus, 3-DCPA is expected to have the highest EL efficiency among the three compounds.

3.2. Optical, thermal and electrical properties

The UV-visible (UV-Vis) absorption spectra and photoluminescence (PL) spectra of the synthesized compounds are shown in Fig. 3, and their optical, thermal and electrical properties are summarized in Table 1. In the solution state, 2-DCPA, 3-DCPA, and 4-DCPA showed similar UV-Vis absorption spectra, with typical vibronic absorption of anthracene and with essentially identical UV_{max} values of 398, 399, and 398 nm, respectively. The PL_{max} values of solution-state 2-DCPA, 3-DCPA, and 4-DCPA were observed to be in the deep-blue region, with values of 439, 445, and 433 nm, respectively. In the film state, 2-DCPA, 3-DCPA, and 4-DCPA also exhibited essentially identical UV_{max} values, of 395, 396, and 395 nm, and showed blue light emission PL_{max} values of 453, 457, and 452 nm, respectively. The full width at half maximum (FWHM) values of the PL_{max} peaks for the three compounds were between 54 and 59 nm and showed only small differences of 3–4 nm compared to solution state. Generally, the film state of a compound with a planar structure causes overlapping of the chromophore due to the short distance between molecules. It also generally causes various transitions and large FWHM values. However, the FWHM values of the peaks of the film states of 2-DCPA, 3-DCPA, and 4-DCPA were all just a little bit different from those of their solution states. The small magnitude of this difference was attributed to the central anthracene core and the carbazole side group being highly twisted, which effectively prevented intermolecular packing and overlapping of the chromophore in the film state. The highly twisted natures of 2-DCPA, 3-DCPA, and 4-

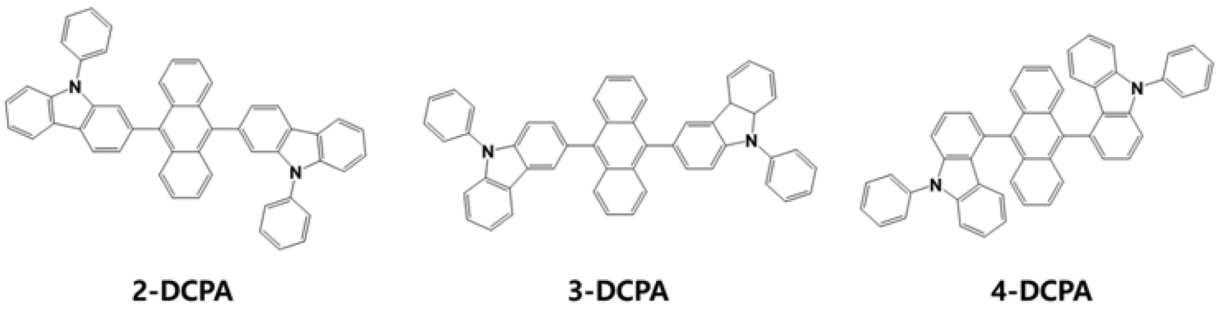

Fig. 1. Chemical structures of the synthesized emitting materials.

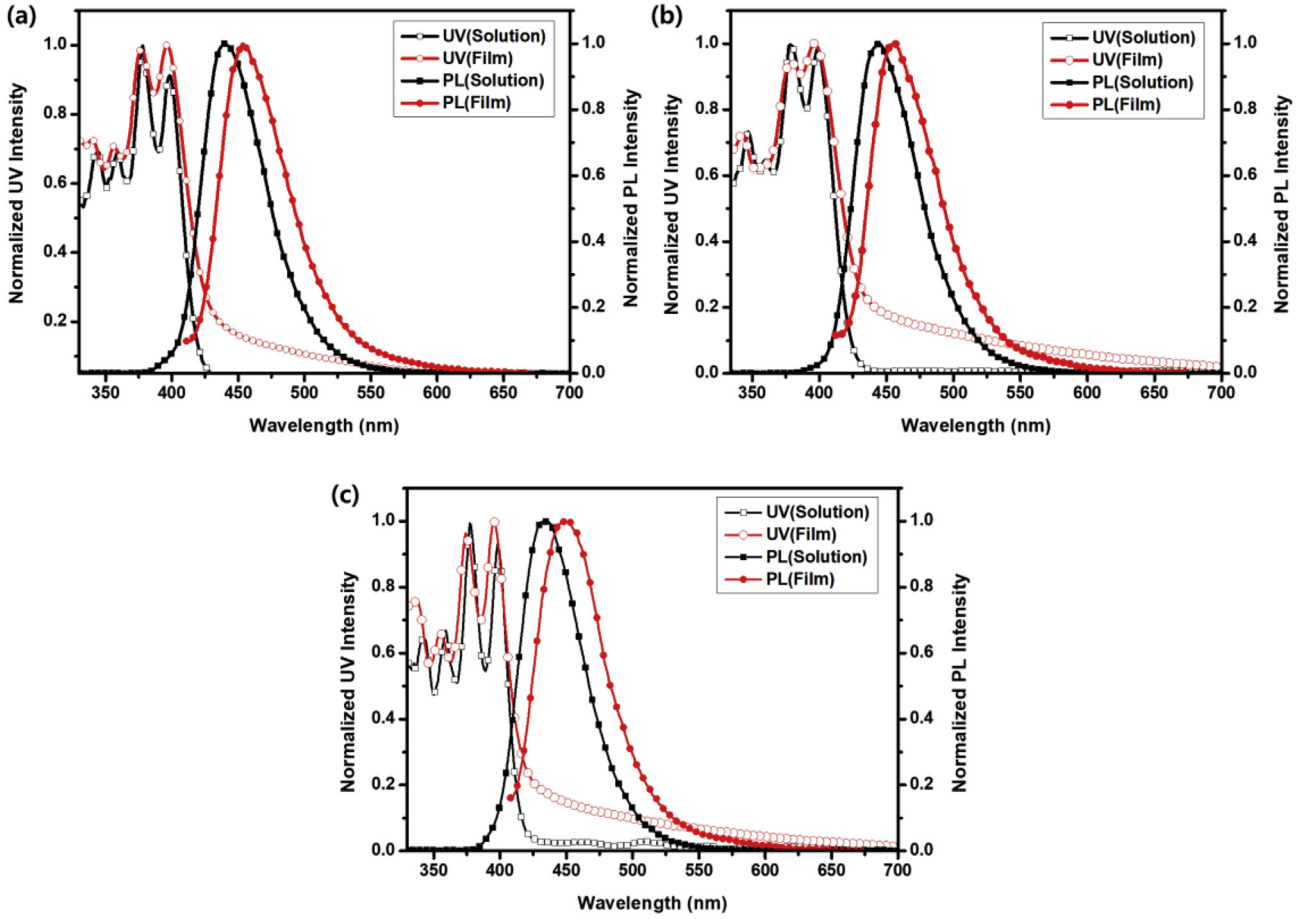

Fig. 3. UV absorption spectra and PL spectra of the three compounds in toluene solutions (1.0 x 10^{-5} M) and thin-film states: (a) 2-DCPA, (b) 3-DCPA, and (c) 4-DCPA.

DCPA were confirmed by performing Gaussian DFT calculations to produce optimized structures for these three compounds, as shown in Fig. 4. The α and β dihedral angles between the anthracene and carbazole moieties of these optimized structures were measured to be between 84.2° and 95.1°, indicative of their highly twisted molecular structures.

Table 1 summarizes the thermal properties of the synthesized compounds as determined using thermal gravimetric analysis (TGA) and differential scanning calorimetry (DSC). The two synthesized compounds of 3-DCPA and 4-DCPA showed not only high T_d values equal to or greater than 412 °C but also high T_m values of at least 273 °C. Molecules with high T_m and T_d values have the advantage that the morphology of the material does not change easily as a result of the heat generated during the operation of the OLED device [18].

Theoretical molecular orbital calculations were carried out using Gaussian09, at the B3LYP/6-31G(d,p) level, to characterize optimized geometries and electron density distributions of the HOMO-1, HOMO, LUMO and LUMO + 1 states of each molecule (Fig. 5).

These calculations produced HOMO and LUMO electron density distributions of 2-DCPA, 3-DCPA, and 4-DCPA showing more electrons located in the anthracene moiety than in the phenyl carbazole moiety, but HOMO-1 and LUMO + 1 electron density distributions showing many electrons distributed in the phenyl carbazole moiety. When the electron density distributions of 2-DCPA, 3-DCPA, and 4-DCPA were considered, they were almost the same as each other. These calculations suggested the main electron transfer from the excited state to ground state after excitation to first occur at the anthracene moiety. Our results indicated anthracene and phenyl carbazole to function as the primary and secondary chromophores, respectively, in each of the three compounds.

Table 1
Optical, thermal and electrical properties of the three compounds.

	Solution[a]			Film on glass[b]			T_d	T_m	HOMO (eV)	LUMO[d] (eV)	Band gap (eV)
	UV_{max} (nm)	PL_{max} (nm)	FWHM[c] (nm)	UV_{max} (nm)	PL_{max} (nm)	FWHM[c] (nm)					
2-DCPA	344,359,377, 398	439	55	339, 355, 376, 395	453	59	433	–	−5.62	−2.62	3.00
3-DCPA	347, 359, 378, 399	445	54	342, 379, 396	457	57	447	273	−5.57	−2.59	2.98
4-DCPA	325, 342, 359, 378	433	55	338, 355, 374, 395	452	59	412	320	−5.65	−2.62	3.03

[a] Toluene solution (1.00 x 10^{-5} M).
[b] Film thickness was 50 nm on the glass.
[c] Full width at half maximum.
[d] HOMO (eV) + Band gap (eV) = LUMO (eV).

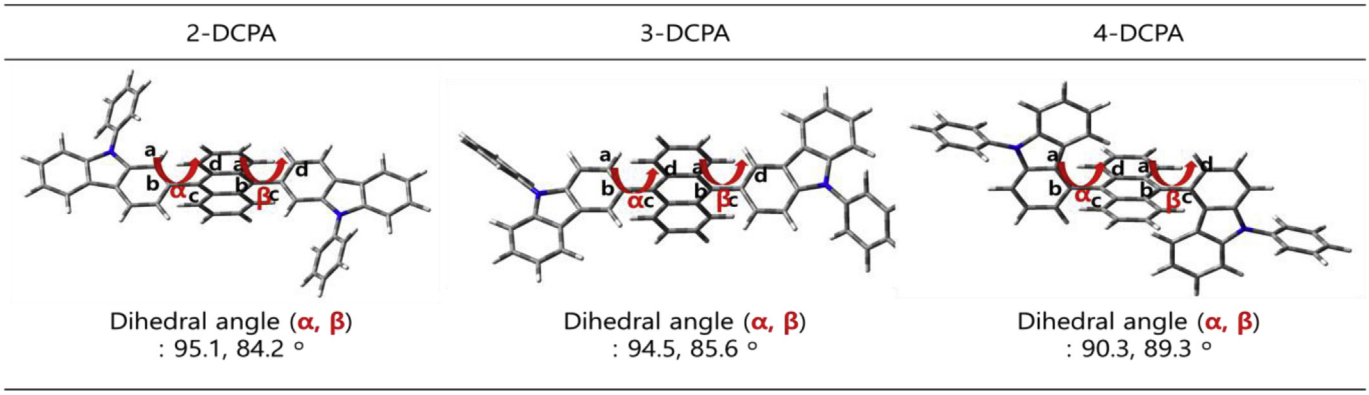

Fig. 4. Optimized structures the synthesized compounds. Dihedral angles were measured from these structures and are noted.

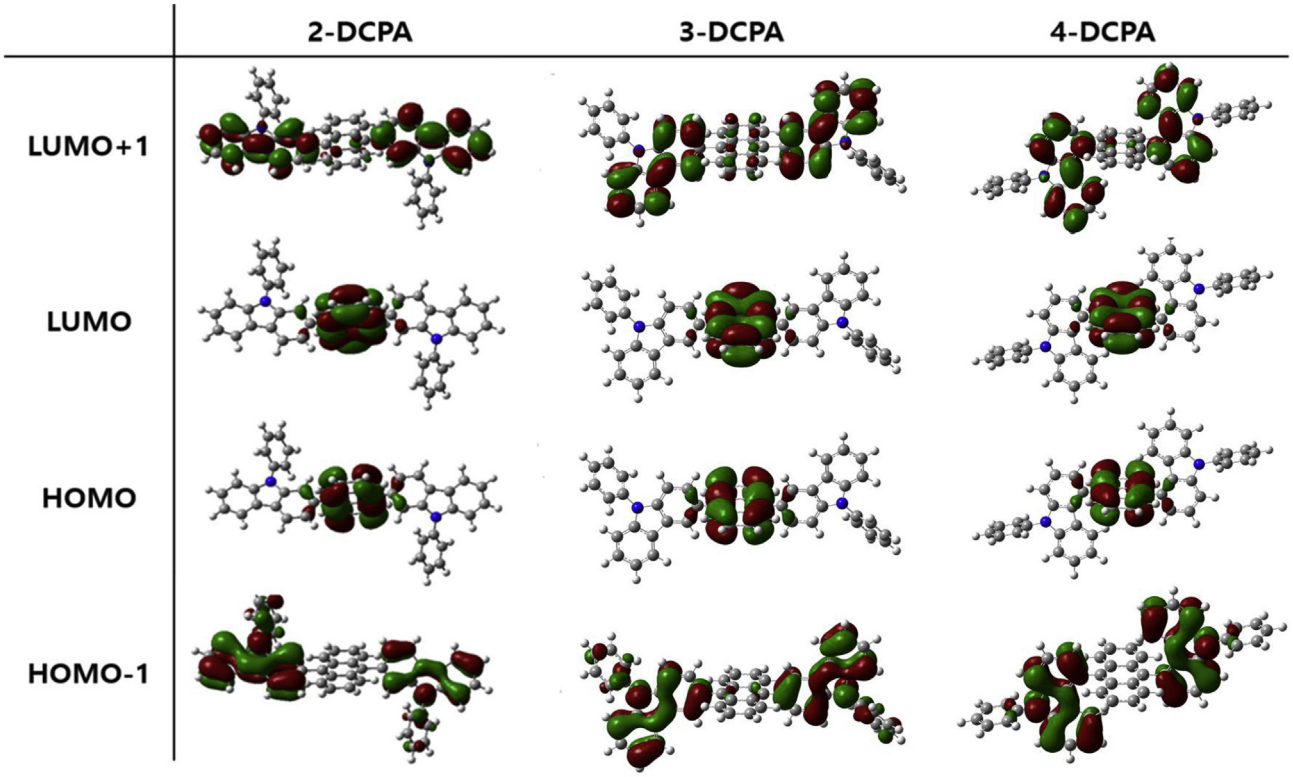

Fig. 5. Electron density distributions of the HOMO-1, HOMO, LUMO and LUMO + 1 states determined from calculations at the B3LYP/6-31G(d,p) level.

Table 2
Absorption frequency and oscillator strength calculated using TD-DFT at the CAM-B3LYP/6-311G(d,p) level for the synthesized compounds.

Compounds	Wavelength (nm)	Oscillator strength	Transition	Contribution (%)[a]
2-DCPA	292	0.2950	HOMO→LUMO + 2	34.0
			HOMO→LUMO + 1	36.0
			HOMO-1→LUMO	4.0
	403	0.6160	HOMO→LUMO	98.0
3-DCPA	255	0.2570	HOMO-3→LUMO + 2	19.0
			HOMO-4→LUMO + 1	11.0
			HOMO-3→LUMO + 1	14.0
			HOMO-1→LUMO	31.0
	366	0.3530	HOMO→LUMO	98.0
4-DCPA	264	0.0750	HOMO-2→LUMO + 2	33.0
			HOMO-1→LUMO + 1	37.0
	367	0.2430	HOMO→LUMO	98.0

[a] Contribution (%) = $(\text{coefficient})^2 \times 2 \times 100$.

Time dependent (TD)-DFT calculations were carried out to further understand the changes in the characteristics of the compounds due to the change in the linkage to the side group. The results of the molecular absorption, oscillator strength and transition level calculations are shown in Table 2. The contribution of the electronic transition using the coefficient values was examined. For each of the 2-DCPA, 3-DCPA, and 4-DCPA compounds, the HOMO →LUMO transition was calculated to be predominant, with a contribution of 98%, and to have oscillator strengths of 0.6160, 0.3530, and 0.2430, respectively, higher than those of the other transitions. These calculations indicated the HOMO→ LUMO transition to be the main electronic transition route and the anthracene with the electron density as main to be the core component of the electronic transition in the molecule. The second highest oscillator strengths calculated for these compounds were 0.2950, 0.2570, and 0.0750, respectively, but corresponded to different transitions for the different compounds, revealing these compounds to have slightly different electronic properties. The contributions of the HOMO-1→ LUMO transition of the three compounds were calculated to be 4%, 31.0%, and 0%, respectively, at 292 nm, 255 nm, and 264 nm. That is, changing the position of the carbazole linked to the anthracene from node to lobe was calculated to result in an increase in the contribution of this transition, which might be helpful for increasing the EL efficiency [19].

These HOMO, LUMO and band gap values are summarized in Fig. 6 and Table 1. The HOMO levels of 2-DCPA, 3-DCPA, and 4-DCPA were found to be very similar, with values of −5.62, −5.57 and −5.65 eV, respectively. The LUMO levels of the synthesized materials were also found to be similar, with values of −2.62, −2.59 and −2.62 eV, respectively, and the band gaps were 3.00, 2.98, and 3.03 eV, respectively. 3-DCPA, having the carbazole lobe position linked to the anthracene, exhibited the smallest band gap of the three compounds, as its PL wavelength was red-shifted.

3.3. Electroluminescence properties

The three new synthesized compounds were each used as an emitting layer (EML) to fabricate, respectively, three non-doped OLED devices, and we measured the EL performances of the devices. Device configuration was as follows: Indium tin oxide (ITO)/4,4′,4″-tris(*N*-(2-naphthyl)-*N*-phenylamino)triphenylamine (2-TNATA) (60 nm)/N,N′-bis (naphthalene-1-yl)-N,N′-bis(phenyl)benzidine (NPB) (20 nm)/synthesized emitting material (35 nm)/Tris-(8-hydroxyquinoline)aluminum (Alq_3) (15 nm)/lithium fluoride (LiF) (1 nm)/Al (200 nm). 2-TNATA was used as a hole injection layer and NPB was used as a hole transport and exciton blocking layer. Alq_3 was used as an electron transport layer. The EL performances of the devices are summarized in Fig. 7 and Table 3.

As shown in Fig. 7 (a), I-V-L curves characteristic of normal diodes were observed. Fig. 7 (c) and (d) show luminance efficiency (LE) and external quantum efficiency (EQE) values of the devices measured at various current density levels in the range of 0–50 mA/cm^2. For each of the three devices, neither efficiency measure decreased much as the current density was increased. 2-DCPA, 3-DCPA, and 4-DCPA yielded EL_{max} values of 453, 457, and 455 nm and corresponding FWHM values of 58, 55, and 59 nm, respectively. The EML in each OLED device effectively prevented close packing of the molecules, with such prevention of packing also suggested from our PL results. 2-DCPA, 3-DCPA, and 4-DCPA yielded CIE y values of 0.12–0.15, i.e., real blue color. These compounds may therefore be applied to mobile phone applications. For the 2-DCPA and 4-DCPA devices, respectively, the LE values were determined to be 2.61 and 1.96 cd/A, the power efficiency (PE) values were 1.32 and 1.00 lm/W, and the EQEs were 2.48 and 2.07%. In the case of the 3-DCPA device, the operating voltage was slightly increased, but this device showed LE, PE, and EQE values, at 2.91 cd/A, 1.44 lm/W, and 2.65%, respectively, higher than those of the other two devices. These high efficiency values for the 3-DCPA device were attributed to 3-DCPA having the lobe position of its carbazole moiety linked to the anthracene core, and the resulting electron donation effect

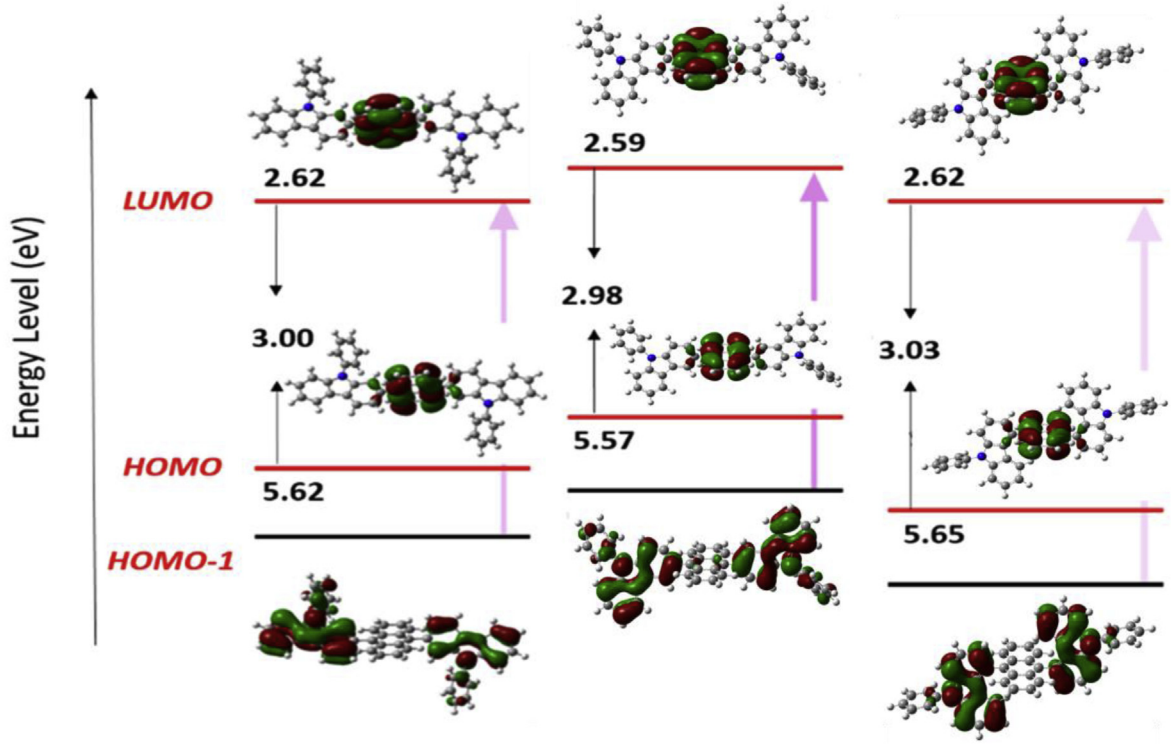

Fig. 6. Plots of calculated molecular orbitals at the LUMO (red top lines), HOMO (red bottom lines), and HOMO-1 (black lines) energy levels of each of 2-DCPA, 3-DCPA, and 4-DCPA. (For interpretation of the references to color in this figure legend, the reader is referred to the Web version of this article.)

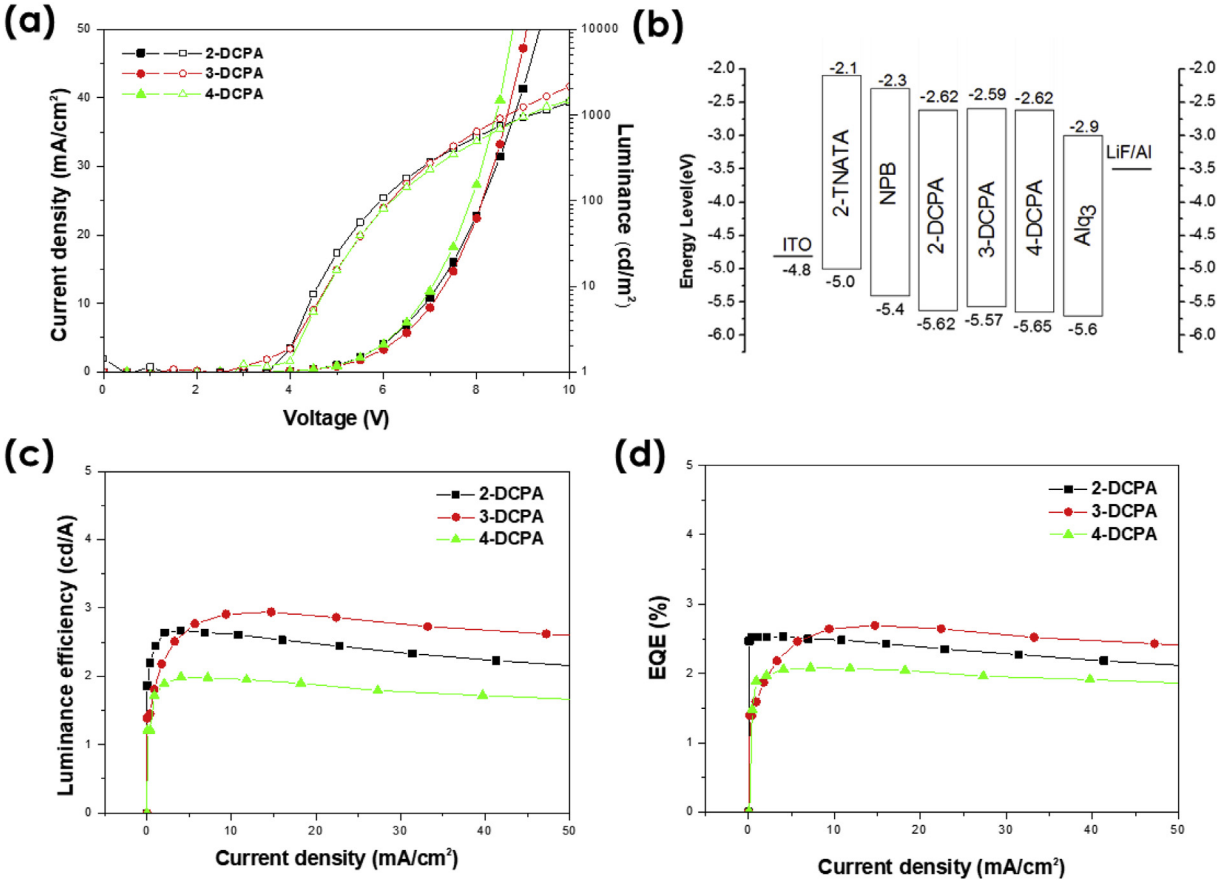

Fig. 7. EL performances of fabricated devices using the synthesized materials as EMLs: (a) I-V (solid symbols) and L-V (opened symbols) curves, (b) energy levels of the organic materials, (c) luminance efficiency versus current density, and (d) external quantum efficiency versus current density.

Table 3
EL performances at 10 mA/cm^2 of non-doped devices made using synthesized materials as emitting layers.

Synthesized compounds	Volt[a] (V)	LE[b] (cd/A)	PE[c] (lm/W)	EQE[d] (%)	CIE[e] (x, y)	EL_{max} (nm)	FWHM (nm)
2-DCPA	6.90	2.61	1.32	2.48	0.16, 0.14	453	58
3-DCPA	7.05	2.91	1.44	2.65	0.16, 0.15	457	55
4-DCPA	6.81	1.96	1.00	2.07	0.16, 0.12	455	59

[a] Operating voltage at 10 mA/cm^2.
[b] Luminance efficiency.
[c] Power efficiency.
[d] External quantum efficiency.
[e] Commission International de l'Eclairage.

of the phenyl carbazole side group. Donation of electrons to a core chromophore generally increases the EL efficiency of the chromophore compound. Y. Park et al. also reported the relationship between lobe position and EL efficiency [19].

In addition, although the PL of the film state well matched the EL data, doped OLED devices were fabricated because the synthesized molecules showed deep-blue PL_{max} wavelengths of 433–445 nm in the solution state. In order to evaluate the performances of the devices, the synthesized compounds were used as dopants and 4,4′-bis(*N*-carbazolyl)-1,1′-biphenyl (CBP) was used as the host material. As shown in Fig. 8, the PL spectrum of the CBP host material and the UV spectra of the three synthesized dopant compounds overlapped well, suggesting there would be no considerable barrier to the transfer of energy from the CBP host material to any of the three dopant compounds. The structures of the devices were ITO/2-TNATA (60 nm-thick)/NPB (20 nm)/CBP: 4wt% synthesized materials (35 nm)/TPBi (15 nm)/LiF (1 nm)/Al (200 nm).

The EL performances of the doped devices using 2-DCPA, 3-DCPA, and 4-DCPA are summarized in Fig. 9 and Table 4. The I-V and L-V curves of the doped devices also showed typical rectifying curve characteristics, and the luminance efficiency at high current density was in each case similar to that at low current density, as shown in Fig. 9 (a) and (c). For the 2-DCPA and 4-DCPA dopant devices, respectively, the LE values were determined to be 1.23 and 0.87 cd/A, the PE values were 0.53 and 0.33 lm/W, and EQE values were 2.21 and 1.74%. The doped device containing 3-DCPA showed an LE of 1.61 cd/A, PE of 0.69 lm/W, and EQE of 1.74%. That is, the doped device using 3-DCPA showed an overall efficiency better than those of the other doped devices, as was found for the non-doped devices. This result was attributed to the structure of the molecule with the linkage made to the lobe position being the most effective for Forster energy transfer from CBP. Electronic states of 2-DCPA and 4-DCPA are basically same, but luminance efficiency was different as 1.23 cd/A and 0.87 cd/A, respectively. It can be explained by the different transition contribution of HOMO to LUMO + 1. As shown in transition case of Table 2, 2-DCPA only had transition from HOMO to LUMO + 1 unlike 4-DCPA, which is related with carbazole moiety. This difference may cause the increment of EL efficiency between 2-DCPA and 4-DCPA. For each of the three materials, the EL_{max} wavelength nearly coincided with the solution PL_{max} wavelength of the dopant material, and a deep-blue color with a wavelength of about 440 nm could be realized. FWHM values of 2-DCPA, 3-DCPA, and 4-DCPA were 55, 54, and 55 nm in solution PL spectra, but when three compounds were used in doped EL device, it was decreased 2–4 nm compared to solution PL. This is not big difference of FWHM as less than 5 nm between spectra of doped EL device and solution PL. It

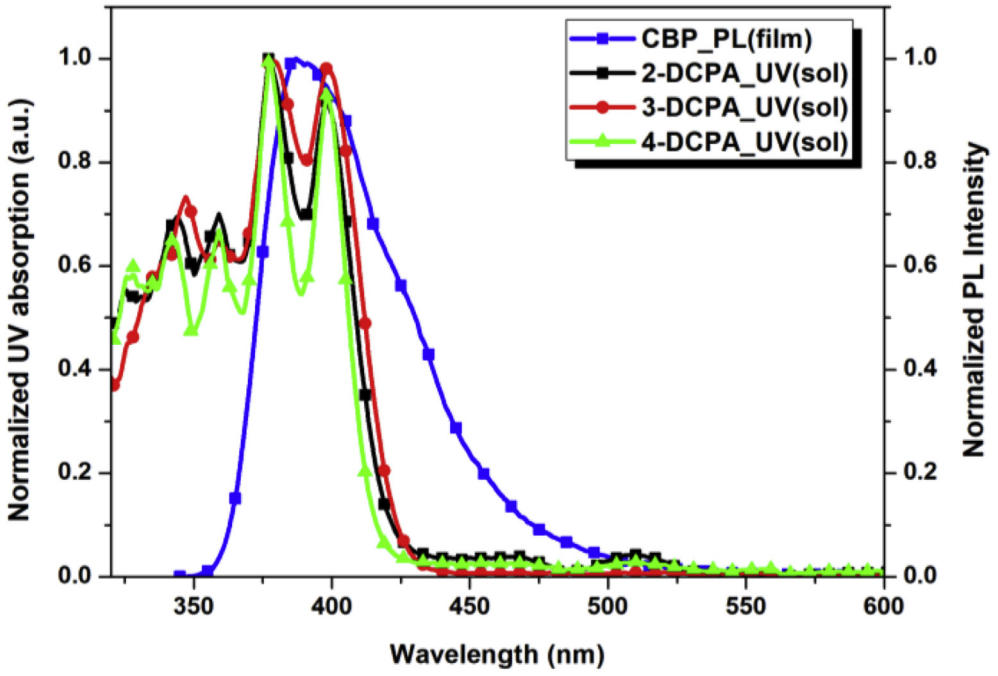

Fig. 8. UV-visible absorption spectra of the synthesized materials (dopant) and PL spectrum of CBP (host).

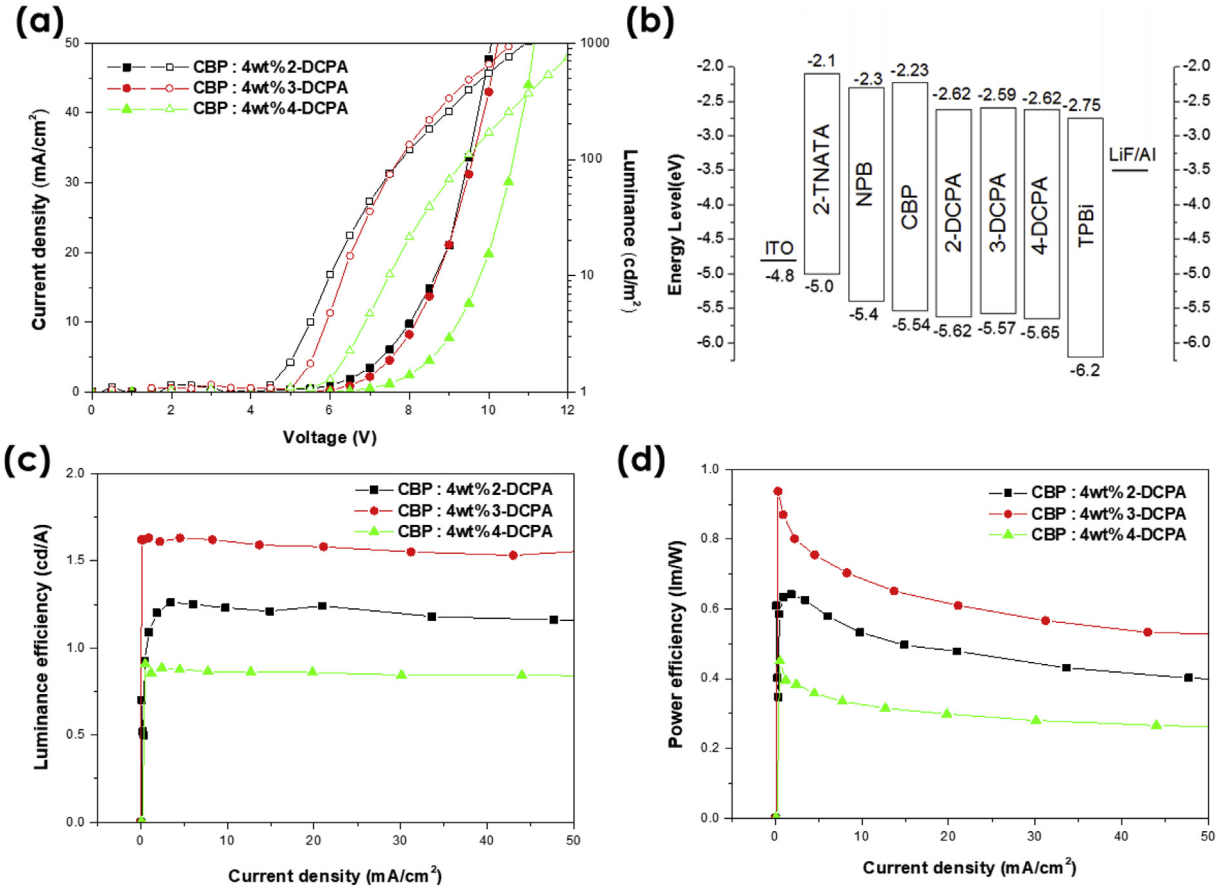

Fig. 9. EL characteristics of doped devices using the synthesized materials as dopants: (a) I-V (solid symbols) and L-V (opened symbols) curves, (b) energy levels of the organic materials, (c) luminance efficiency versus current density, and (d) power efficiency versus current density.

Table 4
EL performances of the doped devices using the synthesized materials as the dopants.

Synthesized compounds	Volt[a] (V)	LE[b] (cd/A)	PE[c] (lm/W)	EQE[d] (%)	CIE[e] (x, y)	EL_{max} (nm)	FWHM (nm)
2-DCPA	8.01	1.23	0.53	2.21	0.153, 0.066	440	52
3-DCPA	8.17	1.61	0.69	2.74	0.150, 0.068	443	50
4-DCPA	9.22	0.87	0.33	1.74	0.153, 0.060	439	53

[a] Operating voltage at 10 mA/cm^2.
[b] Luminance efficiency.
[c] Power efficiency.
[d] External quantum efficiency.
[e] Commission International de l'Eclairage.

could be happened by the effect of solvent polarity. Smaller x and y coordinate values indicate better performance for blue colors. In particular, the y coordinate value must be 0.15 or less for a mobile phone and 0.08 or less for an HD-TV. All of the synthesized materials showed y coordinate values of 0.060–0.068, and can hence be used for HD-TV applications.

4. Conclusions

A new blue light-emitting material was successfully synthesized by linking the node 2- and 4-positions and the lobe 3-position of a carbazole to the anthracene 9- and 10-positions. Non-doped devices made using the synthesized 2-DCPA, 3-DCPA and 4-DCPA showed emission of real blue light. In the case of 3-DCPA, i.e., that with the linkage at the lobe position, the efficiency was 2.91 cd/A and EQE was 2.65%, which showed that the efficiency can be increased by moving the linkage position of the side group to the lobe position. The synthesized material was also used as a dopant to increase color purity of the device; and of the three synthesized materials, 3-DCPA showed the highest efficiency, with a value of 1.61 cd/A, and an EQE of 2.74%, and emitted light in the deep blue region with a CIE (x, y) value of (0.150, 0.068).

Acknowledgements

This research was supported by National R&D Program through the National Research Foundation of Korea(NRF) funded by the Ministry of Science & ICT (No. 2017M3A7B4041699). This research was supported by Basic Science Research Program through the National Research Foundation of Korea(NRF) funded by the Ministry of Education (No. 2017R1D1A1A09082138).

References

[1] Tang CW, Van slyke SA. Organic electroluminescent diodes. Appl Phys Lett 1987;51:913.
[2] Raffaella C, Stefano T, Gianluca G, Hakan U, Antonio F, Michele M. Organic light-emitting transistors with an efficiency that outperforms the equivalent light-emitting diodes. Nat Mater 2010;9:496–503.
[3] Yang L, Shuming C, Jacky WY, Ping L, Ryan TK, Faisal M, Hoi SK, Ben ZT. Tuning the electronic nature of aggregation-induced emission luminogens with enhanced hole-transporting property. Chem Mater 2011;23:2536–44.
[4] Cocchi C, Virgili D, Fattori V, Rochester DL, Williams J. N∧C∧N-Coordinated platinum(II) complexes as phosphorescent emitters in high-performance organic light-emitting devices. Adv Funct Mater 2007;17:285–9.
[5] Jian-Yong H, Yong-Jin P, Fumiya S, So K, Hiroshi K, Hisahiro S, Junji K. Bisanthracene-Based donor–acceptor-type light-emitting dopants: highly efficient deep-blue emission in organic light-emitting devices. Adv Funct Mater 2014;24:2064–71.
[6] Zhang D, Cai M, Bin Z, Zhang Y, Zhang D, Duan L. Highly efficient blue thermally activated delayed fluorescent OLEDs with record-low driving voltages utilizing high triplet energy hosts with small singlet-triplet splittings. Chem Sci 2016;7:3355–63.
[7] Komatsu R, Sasabe H, Seino Y, Nakao K, Kido J. Light-blue thermally activated delayed fluorescent emitters realizing a high external quantum efficiency of 25% and unprecedented low drive voltages in OLEDs. J Mater Chem C 2016;4:2274–8.
[8] Fleetham T, Ecton J, Li G, Li J. Improved out-coupling efficiency from a green microcavity OLED with a narrow band emission source. Org Electron 2016;37:141–7.
[9] Uoyama H, Goushi K, Shizu K, Nomura H, Adachi C. Highly efficient organic light-emitting diodes from delayed fluorescence. Nature 2012;492:234–8.
[10] Giridhar T, Han TH, Cho W, Saravanan C, Lee TW, Jin SH. An easy route to red emitting homoleptic Ir^{III} complex for highly efficient solution-processed phosphorescent organic light-emitting diodes. Chem Eur J 2014;20:8260–4.
[11] Kuei CY, Tsai WL, Tong B, Jiao M, Lee WK, Chi Y, et al. Bis-tridentate Ir(III) complexes with nearly unitary RGB phosphorescence and organic light-emitting diodes with external quantum efficiency exceeding 31 %. Adv Mater 2016;28:2795–800.
[12] Lee S, Kim KH, Limbach D, Park YS, Kim JJ. Low roll-off and high efficiency orange organic light emitting diodes with controlled co-doping of green and red phosphorescent dopants in an exciplex forming co-host. Adv Funct Mater 2013;23:4105–10.
[13] Lee H, Kim B, Kim S, Kim J, Lee J, Shin H, Lee JH, Park J. Synthesis and electroluminescence properties of highly efficient dual core chromophores with side groups for blue emission. J Mater Chem C 2014;2:4737–47.
[14] Shin H, Jung H, Kim B, Lee J, Moon J, Kim J, Park J. Highly efficient emitters of ultra-deep-blue light made from chrysene chromophores. J Mater Chem C 2016;4:3833–42.
[15] Lee J, Jung H, Shin H, Kim J, Yokohama D, Nishimura H, Wakamiya A, Park J. Excimer emission based on the control of molecular structure and intermolecular interactions. J Mater Chem C 2016;4:2784–92.
[16] Wu CL, Chen CT, Chen CT. Synthesis and characterization of heteroatom-bridged bis-spirobifluorenes for the application of organic light-emitting diodes. Org Lett 2014;16:2114–7.
[17] Kim SK, Yang B, Ma Y, Lee JH, Park J. Exceedingly efficient deep-blue electroluminescence from new anthracenes obtained using rational molecular design. J Mater Chem 2008;18:3376–84.
[18] Park YI, Kim B, Lee C, Hyun A, Jang S, Lee JH, Gal YS, Kim TH, Kim KS, Park J. Highly efficient new hole injection materials for OLEDs based on dimeric phenothiazine and phenoxazine derivatives. J Phys Chem C 2011;115:4843–50.
[19] Park YI, Kim S, Lee JH, Jung DH, Wu CC, Park J. New blue-violet emitters based on an indenopyrazine core for OLEDs: effects of the position of m-terphenyl side group substitution on optical and electroluminescence properties. Org Electron 2010;11:864–71.